The Evolution of the Cherenkov Imaging Technique in High Energy Physics

C. Joram

CERN, EP Division, CH-1211 Geneva 23, Switzerland

We give an overview of the Cherenkov imaging technique and discuss its application in experiments at LEP and SLC. Some more recent developments are presented which greatly contributed to the evolution of this technique.

1. Particle identification

Besides the measurement of the specific energy loss dE/dx, the time of flight and the detection of the transition radiation, the Cherenkov imaging technique has become a classic particle identification method. It distinguishes from the other methods by the large momentum band it is able to cover. At LEP and SLC particle identification has played a crucial role as it enabled us to measure many flavour specific parameters of the Standard Model with high precision. In addition to some of the classic methods mentioned above, also the lifetime tag for heavy flavour hadrons, provided by the silicon vertex detectors, developed to an indispensable particle ID tool at LEP and SLC.

New experiments, specialised in CP violation studies in the B-meson system, like BABAR, HERA-B or LHCb, fully rely on the ability to discriminate kaons against pions up to momenta above 100 GeV. The Cherenkov imaging technique is the only technique which can provide this information with the required significance.

This article starts with a brief overview of the basic facts and relations of the Cherenkov imaging technique and a comparison of the characteristics of various photoconverters. We then describe the Cherenkov systems of DELPHI and SLD, discussing their design, operation and performance. We finally review a few exemplary new developments which are considered as important milestones in the evolution of the Cherenkov imaging technique.

2. The Cherenkov imaging technique

The basic principle and the limitations of the Cherenkov imaging technique have been discussed in many articles. Recent treatments of the topic can be found in [1–3]. The basic principle of the Cherenkov imaging technique consists of determining the velocity β of a charged particle by measuring the emission angle θ_C of the Cherenkov radiation. The simultaneous knowledge of β and momentum p allows to derive the rest mass m_0 of the particle and hence its identity

$$m_0 = p/(c\beta\gamma). \tag{1}$$

Cherenkov light is emitted by a fast charged particle ($z \geq 1$) traversing a dielectric medium with a refractive index $n(\lambda) > 1$, if its velocity β exceeds $1/n$. The classical imaging technique intersects the Cherenkov light cone with a (planar) photosensitive detector of appropriate efficiency and granularity. Detectors based on this principle are usually referred to as RICH (Ring Imaging CHerenkov) detectors. From the Cherenkov relation

$$\cos\theta_C = 1/(n\beta) \tag{2}$$

one obtains the threshold velocity and the corresponding momentum

$$\beta_{thr} = 1/n; \qquad p_{thr} = c(\beta\gamma)_{thr}/m_0. \tag{3}$$

For particles approaching $\beta = 1$ the Cherenkov angle saturates at $\theta_C^{max} = \arccos n^{-1}$. The energy spectrum of the emitted Cherenkov photons is flat ($dN_{ph}/dE = const.$) ranging from $E = 0$ to a maximum photon energy E_{max}, corresponding to wavelengths in the UV region, at which the refractive index $n(E) < 1$. The photosensitive detector converts only a small fraction of the Cherenkov light to reconstructed photoelectrons

$$N_{p.e.} = L\sin^2\theta\frac{z^2\alpha}{\hbar c}\int_{E_1}^{E_2}\varepsilon_Q(E)\prod_i\varepsilon_i(E)dE \tag{4}$$

with L being the length of the radiator, $\varepsilon_Q(E)$ the quantum efficiency of the photoconverter and $\varepsilon_i(E)$ describe all other efficiencies involved in the detection and reconstruction process. $\Delta E = E_2 - E_1$ represents the sensitivity range of the photo-converter. From eq. 2 the resolution of a detector is easily derived as

$$\sigma_\beta/\beta = \tan\theta \cdot \sigma_\theta \tag{5}$$

The Cherenkov angular resolution σ_θ depends in first approximation on the single photoelectron resolution and the number of reconstructed photoelectrons.

$$\sigma_\theta = \sigma_{\theta_{p.e.}}/\sqrt{N_{p.e.}} \tag{6}$$

The overall optimisation of the detector resolution requires a compromise between the minimisation of $\sigma_{\theta_{p.e.}}$ and the maximisation of $N_{p.e.}$. While the geometrical contributions to $\sigma_{\theta_{p.e.}}$ can be minimised by taking appropriate measures (detector granularity, optical elements like mirrors, etc.), the chromatic error

$$\sigma_\theta^{chrom} = \frac{1}{n\tan\theta}\frac{dn}{dE}\sigma_E \tag{7}$$

arising from the energy dependence of the refractive index, is practically irreducible unless one limits the sensitive energy window of the photoconverter $\Delta E \propto \sigma_E$, which has obvious adverse effects on $N_{p.e.}$. Alternatively a photoconverter has to be used which allows to work in an energy range where the dispersion dn/dE is small. The performance of many of the existing RICH detectors, which are forced to operate in the UV part of the optical spectrum, is limited by the chromatic error.

2.1. Photodetectors for Cherenkov imaging

The design of a Cherenkov detector and the choice of the material for the radiator and optical elements like windows and mirrors are intimately linked to the choice of the photo-converter. Inspired by the pioneering work of Séguinot and Ypsilantis [4], all large RICH detectors of the first generation, to which we count also DELPHI and SLD, were based on gaseous photo-converters. Small quantities of a photosensitive agent (TMAE or TEA) were admixed to the chamber gas which allowed to detect the photoelectron following an avalanche amplification process in a multi wire proportional chamber. Table 1 gives a comparison of various photo-converters. Particularly in the case of TEA the high photo-ionisation threshold restricts the choice of radiator and window materials. The sensitive energy window is modest due to the absorption of window materials like quartz and limited reflectivity of mirrors. In addition most radiator materials show a significantly increased dispersion dn/dE in the UV compared to the visible range.

Solid photocathodes based on thin CsI films, operated in reflective mode, were developed in the first half of the 1990's and find now applications in several experiments [5–7]. Still bound to the UV region, their main advantage is the precise knowledge of the photon's conversion point, allowing to build detectors with high intrinsic speed (below 100 ns). Comparable speed has been demonstrated in a fast RICH prototype [8] based on TEA which led to a large scale application at CLEO [9].

The use of vacuum photocathodes, like bialkali or multi-alkali antimonide, became possible with the availability of affordable Photo Multiplier Tubes (PMT) and segmented phototubes like Multi Anode PMTs (MAPMT) [10] and Hybrid Photo Diodes (HPD) [11]. These devices allow to operate Cherenkov detectors in the visible and near UV region, giving access to a variety of radiator materials, including aerogel. The physics performance profits from the large sensitive energy window of these devices and the generally reduced optical dispersion of the radiators in this wavelength region.

3. The Cherenkov detectors of DELPHI and SLD

3.1. Principle of operation and design

The RICH detectors of DELPHI [12] and the so-called CRID (Cherenkov Ring Imaging Detector) of SLD [13] follow the same concept: a dual radiator system for coverage of the full momentum band of secondary hadrons ($\approx 0.3-45$ GeV/c), combined with TMAE based photodetection using TPC like gas detectors. While DELPHI comprised Barrel and Forward systems, covering almost the full polar angle range $15^\circ \leq \theta \leq 165^\circ$, only the SLD Barrel CRID was exploited for physics ($40^\circ \leq \theta \leq 140^\circ$). As shown in Figure 1 the tracks crossed first a thin liquid radiator. The generated Cherenkov light propagated through the expansion volume (ca. 15 cm) and was then directly intersected by the photodetector ("proximity focusing"). The tracks continued their path through the gas radiator volume. The light gen-

Table 1
Characteristics of various photo-converters.

type	threshold (eV)	ΔE (eV)	ε_Q	window material	radiator material	speed
TEA[1]	7.45	1.7-2.5[2]	0.3	CaF_2, LiF,...	CaF_2, LiF,...	fast
TMAE[3]	5.6	2	0.35	as above + quartz	as above + quartz + fluorocarbons[4]	slow
CsI	5.9	1.6	0.3	as above	as above	slow
Bi[5]/Multi[6] Alkali	2	4	0.25	as above + glass	as above + aerogel	fast

[1]Triethylamine; [2]Depending on cut-off of the detector gas; [3]Tetrakis(dimethylamine)ethylene; [4] C_4F_{10}, C_5F_{12}, C_6F_{14} in liquid or gaseous form; [5] K_2CsSb; [6] KNa_2CsSb.

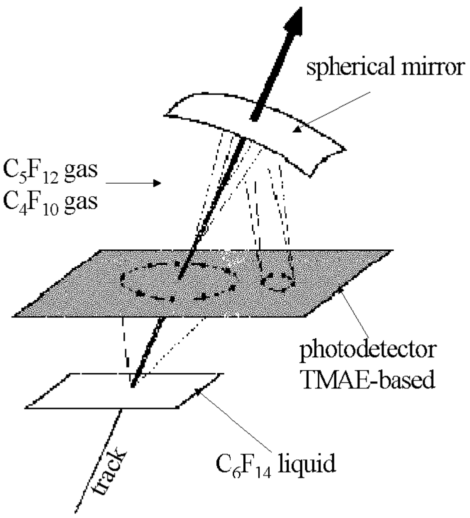

Figure 1. Principle of operation of the DELPHI and SLD Cherenkov detectors.

erated along the track was mirror focused back on the photodetector. Photons emitted under the same angle fell on a ring.

While all systems used a 1 cm thick C_6F_{14} liquid radiator, various media were employed as gas radiator. DELPHI Barrel (DB): ca. 45 cm C_5F_{12} at 1030 mbar; DELPHI Forward (DF): ca. 60 cm C_4F_{10} at atmospheric pressure; SLD Barrel (SB): ca. 45 cm 76% C_5F_{12} and 24% N_2, atm. pressure. While the C_5F_{12} operation of the DELPHI Barrel required active heating to 40°C, the SLD CRID was heated to 35°C and the DELPHI Forward operated at the ambient temperature (30 – 35°C).

The photodetectors were TPC like gas detectors. Each consisted of a driftbox (about 5 cm thick), made out of quartz plates, which was flanged to a MWPC. In the Forward detectors the drift field (1 kV/cm) was orthogonal, in the Barrel systems (ca. 400 V/cm) parallel to the field of the solenoid magnets of DELPHI and SLD. The drift fields were defined by thin metallic strips, which were vacuum deposited on the quartz plates (DELPHI) or by separate etched arrays attached to the quartz plates (SLD). TMAE was admixed to the chamber gas (DF, SB: ethane, DB: 75% methane, 25% ethane) by bubbling the gas through bubblers filled with liquid TMAE. The bubbler temperature determined the vapour pressure and hence the photon conversion length λ_c in the chamber gas. It was maintained at 24°C (DF), 26°C (SB), and 28°C (DB), corresponding to a photon mean free path λ_c between 16 and 21 mm. The MWPC designs and its front-end electronics were optimised for single photon reconstruction. While DELPHI used chambers with a segmented cathode pad readout to provide the second coordinate, SLD employed charge division on 7μm thick carbon wires. In all designs complex systems of blinds suppressed the generation of feedback photoelectrons due to conversion of UV photons originating from the amplification avalanche. The overall resolution for a photoelectron was of the order of 1 mm in all 3 coordinates.

Mechanically the RICH detectors were azimuthally segmented in sectors of 30° (DELPHI) or 36° (SLD). The cylindrical arrangement of Barrel sectors formed a single gas radiator volume and also shared a common potential mid-plane.

3.2. Challenges and problems

The operation of a RICH detector aims at the maximisation of the number of detected photoelectrons combined with an optimum Cherenkov angle resolution. This implies a huge effort in calibration, alignment and monitoring. The safety and integrity of the detector, particularly since it consists to a large extent of fragile quartz components, is however also of utmost importance. A multitude of auxiliary and monitoring systems was required to ensure the stability of the most critical parameters, like refractive indices, transparencies of the radiator media, drift velocities and temperature and pressure in the gas radiator volumes. Large effort was invested in optimising the transparencies of the fluorocarbon liquid and in obtaining high purity TMAE, guaranteeing electron absorption lengths in excess of 10 m. Extensive preventive maintenance and regular checking of all critical operational parameters was equally essential as the day-by-day follow-up of the data quality.

DELPHI

The DELPHI RICH was confronted with two major hardware problems, both concerning only the Barrel part and both consequences of the complex processes which take place when certain polymer and epoxy resin materials are exposed to fluorocarbon liquids over long periods at elevated temperature.

Dimensional changes of wire frames, made out of composite material, which were placed close to the driftboxes on the mirror side, led finally to electrical short circuits between two or more metallic strips on the driftboxes. The consequence were characteristic 3-dimensional distortions of the drift field transforming into radially dependent drift time delays and loss of electrons drifting very close to the quartz plates. Although in total about 40 individual shorts were accumulated over the years, affecting about half of all sectors, no significant degradation of the data quality resulted from it. Thanks to a powerful UV fibre based drift velocity calibration system and the possibility to cross-calibrate space points of charged particles with the DELPHI main tracking detector, most of the shorts could be fully characterised and hence the distortions could be corrected for off-line.

A slowly increasing mixing of the two Cherenkov radiator fluids C_5F_{12} and C_6F_{14} , which was observed in 1993, was traced back to the leakage of the liquid radiator trays inside the gas radiator volume. Due to the shrinkage of Rilsan (Polyamide 11) pipes, used in the trays as internal feedlines, cracks were formed at the glue joints where the pipes were glued into the glass fibre reinforced epoxy resin end pieces. The mixing of the fluids led to a time dependent refractive index of the radiator media. Even more severe, the boiling and dew points of the liquid mixes varied with their composition, which can lead to fatal consequences for the detector hardware. For the 1996 run a semi-industrial scale distillation plant (capacity 150 l/h) was designed and installed. Integrated in the Barrel RICH fluids circulation system and working in a continuous mode, the plant could separate the mixed fluids to a purity of about 99% and so fully compensate the leaks. Stable operational parameters and constant refractive indices contributed significantly to the final physics performance.

SLD

The SLD CRID had to cope with problems related to their single photon detectors. The build-up of polymerised deposits on the anode wires being the result of the combination of a TMAE loaded gas, the very small wire diameter of 7 μm and radiation background from the SLC machine, led to sizeable gain losses (30-40%). However, only a very moderate decrease of the detection efficiency was observed.

Also from the mechanical point of view, the 7 μm carbon wires were a weak point of the design. Broken wires at a rate of one every 4-6 weeks led to a geometrical inefficiency of 5-10%, because the affected chambers had to be switched off until they could be repaired during the next shutdown.

Another phenomenon, namely sporadic emissions of charge in form of single electrons, was attributed to the existence of insulating films on the cathode surface. Accumulation of ions can generate high electric fields at the surface, which give rise to the emission of electrons, a mechanism known as Malter effect. The frequency of this discharges could be reduced to essentially zero by lowering the rate of the UV fibre calibration system.

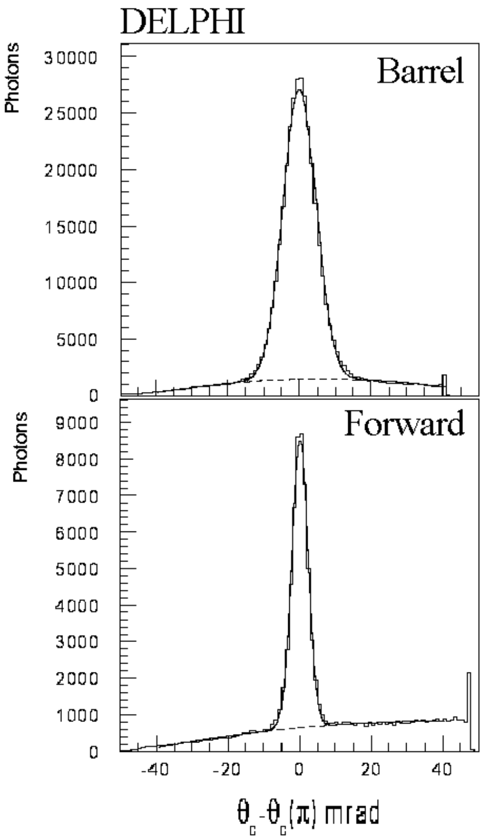

Figure 2. Cherenkov angular resolution per photo-electron of the DELPHI RICH. Top: Barrel gas radiator. Bottom: Forward gas radiator.

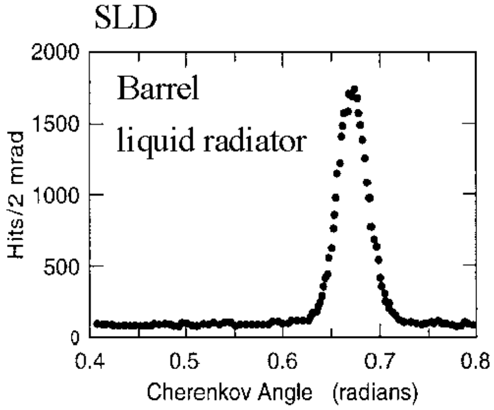

Figure 3. Cherenkov angular resolution per photo-electron of the SLD CRID liquid radiator.

Table 2
Performance[1] of the DELPHI RICH and SLD CRID.

	DELPHI Barrel	DELPHI Forward	SLD CRID
$\sigma_{\theta_{p.e.}}$ gas [mrad]	4.6	2.5	4.5
σ_θ gas [mrad]	1.5	1.2	
$N_{p.e.}$ gas	8.3	5.2	10
$\sigma_{\theta_{p.e.}}$ liquid [mrad]	13.3	11.4	15[2]
σ_θ liquid [mrad]	5.2	5.0	
$N_{p.e.}$ liquid	18.6	7.9	16.5

[1] Measured in simple topologies like $Z^0 \to \mu^+\mu^-$.
[2] Measured at track dip angle $\theta_t = 0$.

3.3. Performance

DELPHI and SLD proved that the RICH concept can be applied to large 4π geometries and that complex RICH systems can be operated at constantly high physics performance over many years. The achieved single photon and "ring" resolutions as well as the number of reconstructed photoelectrons are summarised in table 2. These numbers have been obtained in events with simple topologies, like $Z^0 \to \mu^+\mu^-$ (see figures 2 and 3). While the number of reconstructed photoelectrons is in good agreement with M.C. expectations, both experiments could not fully achieve the predicted Cherenkov angle resolution for the liquid radiators. It should be noted that the resolution of the liquid radiator system is very sensitive to alignment and tracking errors, but also to the precise value of the optical dispersion of C_6F_{14}. The "di-muon" performance, which is often taken as benchmark figure for comparisons, could not be fully maintained in dense hadronic jet topologies, where overlapping rings and background from ionisation caused additional problems to the pattern recognition algorithms. Together the DELPHI RICH and the SLD CRID have operated for almost 15 years. Many physics results reported in these proceedings strongly relied on the hadron identification provided by these detectors. When talking about the *legacy of LEP and*

SLC, the Cherenkov imaging technique has made a distinct and remaining contribution to it.

4. New developments

RICH detectors developed and built for experiments in the post LEP and SLC era faced new requirements. Most of the applications demand a drastically increased readout speed to cope with short bunch crossing intervals, and for some experiments particle ID has to be provided over an extended momentum band. As sketched in chapter 2.1, during the last decade detectors have been built or are currently under development which make use of fast TEA based photoconverters, solid CsI photocathodes, or vacuum phototubes. We have to restrict our discussion to a few exemplary detectors and projects, which introduced new concepts in terms of optics, photodetectors or radiator materials.

4.1. The DIRC at BABAR

The DIRC (Detection of Internally Reflected Cherenkov light) detector, installed in the BABAR detector [14,15] at PEP-II, is an outstanding example as it not only featured for the first time a large photosensitive surface equipped with vacuum photomultiplier tubes, but also introduced a completely new optical concept. The DIRC principle inverts the classical RICH principle by collecting and imaging only the light which is total internally reflected, rather than the transmitted light. As the principle relies on the intrinsically high reflection coefficient in the total internal reflection, it is limited to solid radiators and therefore to low and intermediate energy applications.

A significant fraction of the Cherenkov light emitted in the quartz radiator bar ($n \approx 1.47$) is trapped inside the quartz bar and propagates via total internal reflection[1] to the photosensitive plane while the magnitude of the emission angles is conserved. The Cherenkov images obviously decomposes due to the left/right ambiguities from the last reflection in the bar, a phenomenon which is taken care of by the reconstruction software without loss of performance. In total 144 fused silica bars ($1.7 \times 3.5 \times 490$ cm^3), arrayed as a 12-sided polygon, form the radiator of the DIRC. The photosensitive plane, separated from the radiator by a 120 cm long standoff box filled with water for refractive index matching, is equipped with about 11,000 standard PMTs (28 mm Ø), arranged in a close packed array. The fact that the standoff box could be placed outside the active volume of the BABAR detector, i.e. only the radiator arrangement contributes to the material budget, makes the DIRC concept particularly attractive for low energy applications. With a single photoelectron resolution $\sigma_{\theta_{pe}} = 9.8$ mrad (7 mrad from PMT size, 5.4 mrad chromatic error) and an average of about 30 reconstructed photoelectrons the DIRC provides excellent π/K separation on a 4σ level up to 3 GeV/c.

The DIRC is intrinsically a 3-D device: in addition to the coordinates of the photon in the detection plane (x_p, y_p), the arrival time of the photon t_p is measured. The pathlength of the photon L_p can be calculated from (x_p, y_p) and the particle trajectory. With a time resolution of $\sigma_t \approx 1.7$ ns this represents an efficient way to suppress background. The photon propagates from the emission point to the detection plane with the group velocity v_g.

$$t_p = \frac{L_p}{v_g} \qquad v_g = \frac{c}{n(\lambda) - \lambda \frac{dn}{d\lambda}} \tag{8}$$

Apart from the intrinsic resolution of the photodetectors $\sigma_t^{intr.} \approx 1.6$ ns, which is dominating at the BABAR DIRC, also the dispersion of v_g contributes to the time resolution. Exploiting this relatively strong dispersion can lead to a "super" DIRC [16]. Detailed calculations shows that with an intrinsic time resolution of 150 ps the wavelength of the photon can be derived from eqn. 8 with a precision of $\sigma_\lambda \approx 10 - 50$ nm reducing the chromatic error to well below 0.2 mrad. To profit from this gain also the geometrical error, which is currently limiting the DIRC performance, needs to be strongly reduced. Very fast and highly granular photodetectors (2×2 mm^2) could push the DIRC performance to a 4σ π/K limit at 6 GeV/c. A possible design is shown in Fig.4.

4.2. The RICH detectors of LHCb

The future single arm spectrometer LHCb includes two RICH detectors [17] for π/K separation in the momentum range 1-150 GeV/c. In addition to gaseous radiator media (CF_4, C_4F_{10}) the use of a 5 cm thick aerogel radiator will enhance the performance in the low momentum range.

[1] critical angle for total internal reflection $\theta_{crit.} \approx 49°$, corresponding to the Cherenkov angle for a particle with $\beta \approx 0.93$

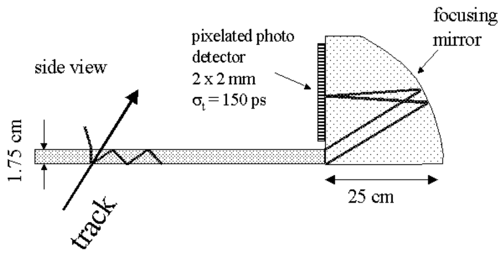

Figure 4. A DIRC design with focusing mirror and highly segmented photodetectors.

Aerogel as radiator material

Aerogel is a colloidal form of quartz. Recently improved optical characteristics led to its first demonstration as a RICH radiator medium [18] and to its application in the RICH of HERMES [19]. The refractive index of aerogel can be tuned during the delicate manufacturing process in a certain range (1.01 - 1.1) and lies in the gap between gaseous and liquid or solid radiator materials. In case of LHCb a value of n = 1.03 is foreseen. However, light suffers coherent Rayleigh scattering from the micro bubbles. The unscattered fraction of Cherenkov light which was uniformly emitted over the length L is given by

$$f_{unscattered} = \frac{\lambda^4}{CL}(1 - e^{-CL/\lambda^4}) \tag{9}$$

with C the clarity coefficient (0.005 – 0.01 μm^4/cm) This strong λ dependence restricts the use of aerogel to the visible and near UV part of the optical spectrum. The LHCb RICH counters therefore need to be equipped with visible light photodetectors. The required Cherenkov angular resolution translates to a granularity of 2.5×2.5 mm^2 over a total photosensitive area of 2.9 m^2.

4.3. Novel segmented photodetectors

Wire chambers combined with TEA, TMAE or CsI, allow to build finely segmented single photon detectors in the UV range. Spatial resolution in the mm range and below are relatively easy to achieve. Until recently arrays of classical vacuum photomultiplier tubes represented the only way to obtain the analogue performance for visible light. The high cost of thousands of individual tubes and the limited segmentation (of the order of a cm) were serious obstacles for their use in Cherenkov detectors. Apart from MAPMTs and HPDs, which will be discussed in more detail below, also more exotic devices shall be mentioned here: Avalanche Photo Diodes, now available as finely segmented arrays [22], Silicon Photomultiplier (SiPM) [23], Visible Light Photon Counters (VLPC) [20,21], Tungsten Edge Sensor (TES) [24]. All these devices have very appealing characteristics like high Q.E. or insensitivity to magnetic fields, however other features, like thermal noise, low intrinsic speed or impractical operational conditions, make their use in Cherenkov detectors unlikely in the near future.

4.3.1. Multi Anode Photomultiplier Tubes

The spatial sensitivity of a MAPMT is based on its segmented dynode structure which consists of a package of micro machined metal meshes defining independent amplification columns. The individual anodes are usually arranged in a matrix geometry. This technology allows to achieve a segmentation of 2×2 mm^2 without significant cross talk. Quantum efficiency and gain are comparable to a standard PMT. Equipped with lens systems to reduce geometrical inefficiencies, 16 channel MAPMT (Hamamatsu R5900-16) are used as focal plane detectors in the HERA-B RICH [25]. While the first generation of MAPMTs was limited to small sizes and suffered from significant dead zones, large 'flat panel' devices have been developed by Hamamatsu and are expected to be soon commercially available. The drawbacks of the metal mesh technology are the channel-to-channel gain variation (factor 3 in recent models), the modest pulse height resolution which is intrinsic to the cascade amplification process with low individual amplification steps, and an expressed sensitivity to transverse magnetic fields.

4.3.2. Hybrid Photo Diodes

The HPD concept replaces the cascade amplification mechanism of a PMT by a single dissipative step. As shown in Fig. 5 the accelerated photoelectrons bombard a silicon sensor and penetrate it to a depth of a few μm. The number of created electron-hole pairs per photoelectron, i.e. the gain of the device, is in first approximation given by

$$G = \Delta V / W_{e-h} \tag{10}$$

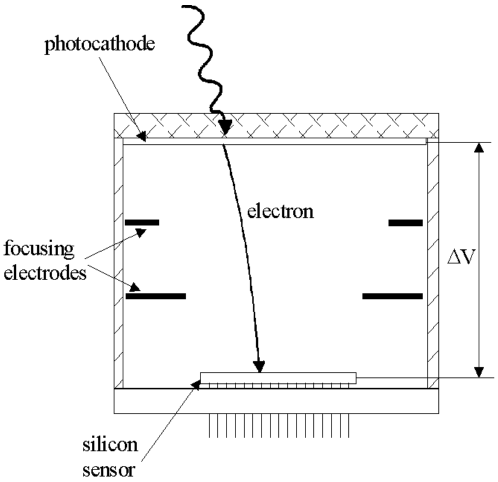

Figure 5. Principle of operation of a HPD.

With W_{e-h} = 3.6 eV, the average energy needed for the creation of a single electron-hole pair in silicon, and a potential difference ΔV = 20 kV a gain of about 5000 is achieved. The statistical fluctuation of the number of charge carriers is in general negligible compared with the pedestal noise spread of the electronic detection chain. Spatial sensitivity is obtained by segmenting the Si wafer in individual diodes. The electron optics of the tube ('point spread function') and charge sharing effects between very small ($\approx$ 50 μm) pixels represent the only intrinsic limits. For large channel numbers the (multiplexed) readout electronics can be incorporated in the vacuum envelope. R&D work for the LHCb RICH counters led to the development of two HPD detectors.

The 80 mm Pixel HPD

The 80 mm diameter HPD [26], which is the baseline photodetector for the LHCb RICH counters, makes use of the cross focusing technique. The image from the 72 mm active diameter photocathode (multialkali) is demagnified by a factor $\approx$ 5 onto a silicon sensor consisting of 10240 pixels of 50 $\times$ 500 μm^2 each. The tube operates at a cathode voltage of -20 kV. A binary readout chip is bump bonded to the pixel array. Groups of 10 pixels are electronically OR-ed to form a super pixel of 500 $\times$ 500 μm^2. The tube was developed in collaboration with the company DEP. The chip was designed and tested together with the ALICE tracking group. The first tube with an enclosed ALICE-LHCb pixel chip is currently under test. The remaining crucial points are the demonstration of 40 MHz operation combined with high single photoelectron detection efficiency and low noise.

The 5-inch Pad HPD

The Pad HPD [27] has a total diameter of 5 inches (127 mm) and is equipped with a bialkali photocathode. Ring electrodes produce a fountain-like electrostatic field geometry, which results in a linear demagnification of 2.7 over the full active diameter of 114 mm. The silicon sensor (50 mm Ø) is segmented in 2048 pads of 1 $\times$ 1 mm^2 size, read out by analogue electronics chips wire bonded to the Si sensor. The tube is developed and built in a dedicated fabrication plant at CERN. An advantage of this concept is the versatility in the choice of the electronics. During the LHCb R&D phase several prototypes have been built and successfully tested with chip sets with different shaping time (VA2/3, τ = 1 − 3 μs; VAPRIME, τ =350 ns). Currently prototype tubes with self triggering VATAGP electronics are under preparation, which aim at applications in cosmic ray physics and medical imaging.

4.4. Summary

The Cherenkov imaging technique has become a well established particle identification method. Physics at LEP and SLC has greatly profited from the complex but reliable Cherenkov detectors. New developments in the field of photodetectors, radiator materials and optical concepts led to improved performance and will further widen the range of applications.

REFERENCES

1. J. Séguinot and T. Ypsilantis, *Nucl. Instr. Meth. A343 (1994)* 1
2. T. Ypsilantis and J. Séguinot, *Nucl. Instr. Meth. A343 (1994)* 30
3. P. Glässel, *Nucl. Instr. Meth. A433 (1999)* 17
4. J. Séguinot and T. Ypsilantis, *Nucl. Instr. Meth. 142 (1977)* 377
5. G. Baum et al. *Nucl. Instr. Meth. A433 (1999)* 207
6. Tech. Design Report, CERN/LHCC 98-19

7. K. Zeitelhack et al., *Nucl. Instr. Meth. A433 (1999)* 201
8. J.L. Guyonnet et al,. *Nucl. Instr. Meth. A343 (1994)* 179
9. R.J. Mountain et al., *Nucl. Instr. Meth. A433 (1999)* 77
10. Y. Yoshizawa and J. Takeuchi *Nucl. Instr. Meth. A387 (1997)* 33
11. C. Joram, *Nucl. Phys. B Proc. Suppl. 78 (1999)* 407
12. W. Adam et al., *Nucl. Instr. Meth. A433 (1999)* 68
13. K. Abe at al., *Nucl. Instr. Meth. A433 (1999)* 74
14. Tech. Design Report, SLAC-REP-95, 457, 1997
15. I. Adam et al. *Nucl. Instr. Meth. A433 (1999)* 121
16. B. Ratcliff, SLAC-PUB-8989, 2001
17. Tech. Design Report, CERN/LHCC 2000-037
18. R. De Leo et al., *Nucl. Instr. Meth. A401 (1997)* 187
19. P. Carter, *Nucl. Instr. Meth. A433 (1999)* 392
20. M.D. Petroff at al., Appl. Phys. Lett. *51* 6 (1987)
21. D. Lincoln, *Nucl. Phys. B Proc. Suppl. 78 (1999)* 281
22. http://www.rmdinc.com
23. G. Bondarenko at al., *Nucl. Instr. Meth. A 442 (2000)* 187
24. B. Cabrera et al., Appl. Phys. Lett. *73*, 735 (1998)
25. S. Korpar et al., *Nucl. Instr. Meth. A433 (1999)* 129
26. T. Gys *Nucl. Instr. Meth. A465 (2001)* 240
27. A. Braem et al., *Nucl. Instr. Meth. 442 (2000)* 128